2021 60th IEEE Conference on Decision and Control (CDC)
December 13-15, 2021. Austin, Texas

Higher-Order Spatial Iterative Learning Control for Additive Manufacturing

Zahra Afkhami, David Hoelzle, Kira Barton

2021 60th IEEE Conference on Decision and Control (CDC) | 978-1-6654-3659-5/21/$31.00 ©2021 IEEE | DOI: 10.1109/CDC45484.2021.9682875

nopageno *Abstract*— **This paper presents a higher-order spatial iterative learning control (HO-SILC) framework for heightmap tracking of 3D structures that are fabricated by additive manufacturing (AM) technology. In the literature, first-order spatial ILC (FO-SILC) has been used in conjunction with additive processes to regulate single-layer structures. However, ILC has undeveloped potential to regulate AM structures that are fabricated by the repetitive addition of material in a layer-by-layer manner. Estimating the appropriate feedforward signal in these structures can be challenging due to iteration varying system parameters. In this paper, HO-SILC is used to iteratively construct the feedforward signal to improve device quality of 3D structures. To have a more realistic representation of the additive process, iteration varying uncertainties in the plant dynamics and non-repetitive noise in the input signal are included. We leverage the existing FO-SILC models in the literature and extend them to a HO-SILC framework that incorporates data available from a previously printed device, as well as multiple previously printed layers to enhance the overall performance. Subsequently, the monotonic and asymptotic stability conditions for the nominal HO-SILC algorithm are illustrated.**

I. INTRODUCTION

There is a growing interest in additive manufacturing (AM) technologies due to their potential for simplified processing and freedom to design. Through AM, a 3D device is generated by sequential addition of material on the surface [1]–[3]. The performance of such devices depends on the uniformity and consistency of the layers [2]. However, the lack of real-time monitoring devices that can capture *in situ* measurements has been a challenge for most AM systems. Additionally, AM processes are innately iteration varying, and the system parameters and plant dynamics change iteratively. Thus, the behavior of the printed layer depends on topology interactions from previous layers, which vary in real-world applications. Control methods that leverage the iterative nature of these processes in the presence of disturbances are needed.

Iterative Learning Control (ILC) is a powerful technique that has been used to achieve accurate output tracking of a reference trajectory over a short number of iterations [4]. Most ILC literature focuses on first-order ILC (FO-ILC) where the feedforward signal comes from the most recent iteration. However, FO-ILC loses performance when uncertainties are high. To improve performance and robustness to iteration varying uncertainties, higher-order ILC (HO-ILC) has been developed where the feedforward signal is synthesized from multiple past-history data [5]–[10].

Recent work in the literature has focused on extending temporal ILC to the spatial domain such that system parameters are defined based on spatial coordinates [11]. Spatial ILC (SILC) has been demonstrated for topology control for predominantly single-layer material deposition with AM systems [11]–[13].

Our previous work introduced a FO-SILC framework [14] that considered in-layer and layer-to-layer dynamics to achieve uniform layers in multi-material 3D-structures. A limitation of this framework stems from the additive process. Error accumulation over multiple layers leads to increased iteration varying system behavior [15]. However, the FO-SILC framework in [14] only considers current layer errors, $\Delta e_{l,j}(x,y)$ rather than total error within the system, $e_{l,j}(x,y)$.

In this manuscript, we extend our earlier work in [14] towards the development of a higher order SILC (HO-SILC) framework that encompasses model uncertainties and spatially varying dynamics from multiple layers of a 3D printed component. The proposed HO-SILC framework incorporates **vertical learning** through the combined effect of previous layer spatial dynamics and layer-to-layer learning, and **horizontal learning** from device-to-device. The proposed HO-SILC differs from traditional HO-ILC frameworks due to the 2D aspect of the learning. HO-SILC incorporates learning over two axes; along the device-axis (j horizontal) and over multiple iterations in the layer axis (l vertical). The contributions of this work are:

1) A HO-SILC framework for 3D AM structures that combines device-to-device and layer-to-layer learning while considering iteration varying spatial dynamics.
2) A strategy for converting HO-SILC to a FO-SILC format for analysis.
3) The development of learning filter designs that incorporate stability considerations.

Simulation results using a model of an electrohydrodynamic jet (e-jet) printing process are used to demonstrate the feasibility of the proposed HO-SILC framework in AM processes.

II. PRELIMINARIES

In this Section, preliminary notations and definitions that will be used in the upcoming Sections will be defined.

This material is based upon work supported by the National Science Foundation under Grant No. CMMI-1727894. Any opinions, findings, and conclusions or recommendations expressed in this material are those of the authors and do not necessarily reflect the views of the National Science Foundation.

K. Barton and Z. Afkhami are with the Department of Mechanical Engineering, University of Michigan, Ann Arbor, MI 48109, USA. zafkhami@umich.edu

D. Hoelzle is with the Department of Mechanical and Aerospace Engineering, The Ohio State University, Columbus, OH 43210, USA.

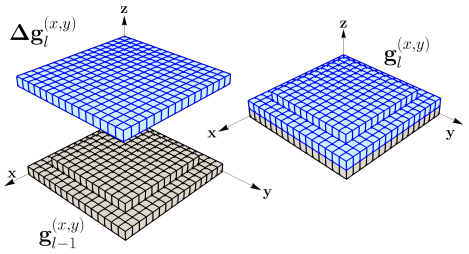

Fig. 1: Schematic of AM spatial dynamics described in Eq. (1).

A. Notation

The finite set of $\mathbb{Z}_n$ for an odd and positive integer n is defined as $\mathbb{Z}_n \triangleq \{\frac{1-n}{2}, \frac{3-n}{2}, ..., \frac{n-3}{2}, \frac{n-1}{2}\}$, with $\mathbb{Z}_1 \triangleq \{0\}$. A vectorization operator $\nu(.)$ can be applied to a matrix, $P \in \mathbb{R}^{m\times n}$, to convert it into a column vector form (denoted by a bold variable), $\mathbf{P} \in \mathbb{R}^{mn\times 1}$, given as

$$\mathbf{P} \triangleq \nu(P) = vec(P^T).$$

where $vec(.)$ is the conventional column-wise vectorization operator. The Frobenius norm of a matrix $P \in \mathbb{R}^{m\times n}$ is equal to the l_2 norm of the vectorized matrix, $\|P\|_F = \|\nu(P)\|_2$.

B. Definitions

- $circ(p_1, p_2, ..., p_n)$ is defined as a block circulant matrix with square submatrices of the same size, $p_1, p_2, ..., p_n$, where n is an odd number. The ith block of the middle column in $circ(p_1, p_2, ..., p_n)$ is always p_i [13].
- A matrix is said to be block circulant with circulant blocks (BCCB) if it is defined as

$$\mathbf{H} \triangleq circ(\mathbf{H}_{\frac{1-M}{2}}, \mathbf{H}_{\frac{3-M}{2}}, ..., \mathbf{H}_{\frac{M-1}{2}}) \in \mathbb{R}^{MN\times MN}$$
$$\mathbf{H}_i \triangleq circ(h(i, \frac{1-N}{2}), h(i, \frac{3-N}{2}), ..., h(i, \frac{N-1}{2})), \in \mathbb{R}^{N\times N}$$

where $h(x,y)$ is a discrete function with $(x,y) \in \mathbb{Z}_M \times \mathbb{Z}_N$.

III. General Iteration Varying Systems

Models describing the sequence of material addition and heightmap evolution (illustrated in Figure 1) have been introduced in [11] and [16]. In these models, the printed topology at layer l, $g_l(x,y)$, is the sum of previous layer topology, $g_{l-1}(x,y)$, and newly added material, $\Delta g_l(x,y)$. The general simplified system model can be described using the following 2-D convolution format [16],

$$g_l(x,y) = g_{l-1}(x,y) + \sum_{\substack{m\in\mathbb{Z}_M \\ n\in\mathbb{Z}_N}} h_{l-1}^{(m,n)}(x-m, y-n) * f_l(m,n), \quad (1)$$

where f_l is the input signal that denotes the droplet size (cube root of droplet volume [16]). $h_{l-1}^{(m,n)}$ describes the spreading behavior of a printing material on the neighboring coordinates when an input signal with magnitude one is applied at coordinate $(m,n) \in \mathbb{Z}_M \times \mathbb{Z}_N$ and layer $l-1$. The system defined in Eq. (1) can be converted to the lifted-form through the use of the vectorization operator as described in [11]. For brevity, we present the lifted form of Eq. (1) in the following equation,

$$\mathbf{g}_l = \mathbf{g}_{l-1} + \mathbf{H}(\mathbf{g}_{l-1})\mathbf{f}_l, \quad (2)$$

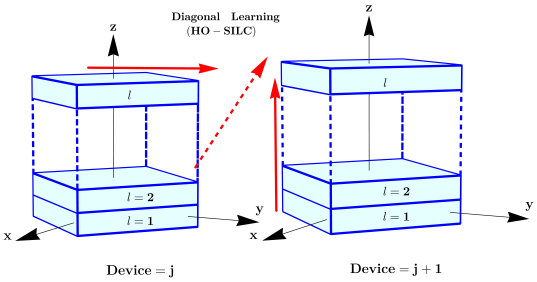

Fig. 2: **HO-SILC**: learning occurs in horizontal direction from a previous device and vertical direction from previous layers and topology. l denotes layer index and j denotes iteration or device index.

with $\mathbf{f}_l \triangleq \nu(f_l(x,y)) \in \mathbb{R}^{MN\times 1}$, $\mathbf{g}_l \triangleq \nu(g_l(x,y)) \in \mathbb{R}^{MN\times 1}$, and $\mathbf{H}(\mathbf{g}_{l-1}) \in \mathbb{R}^{MN\times MN}$ is the plant matrix associated with the interval impulse response $h_{l-1}^{(m,n)}$. We will use $\mathbf{H}_{l-1}$ instead of $\mathbf{H}(\mathbf{g}_{l-1})$ for brevity. Note that $\mathbf{H}_{0,j}$ denotes that deposition of material at the first layer ($l=1$) on the substrate. For a general additive manufacturing process, we are interested in controlling the heightmap increment with respect to the previous layer described as,

$$\Delta\mathbf{g}_l \triangleq \mathbf{g}_l - \mathbf{g}_{l-1} = \mathbf{H}_{l-1}\mathbf{f}_l, \quad (3)$$

The following assumptions are considered for the AM process described in Eq. (2),

- $\mathbf{A}_1$: The plant spatial dynamics are causal in the temporal and noncausal in the spatial domain, meaning that the applied input at a given position will affect the output in the advanced layers and surrounding coordinates [11], [17].
- $\mathbf{A}_2$: The plant is considered bounded input, bounded output (BIBO) stable, meaning that there exist positive finite scalars ξ and ζ such that given a bounded input, $\|\mathbf{f}_l(x,y)\| < \xi$, the resulted output will always be bounded, $\|\mathbf{g}_l(x,y)\| < \zeta$, $\forall (x,y) \in \mathbb{R}^{M\times N}$.
- $\mathbf{A}_3$: The heightmap increments obey scalar multiplication and linear superposition. Therefore, the model in Eq. (1) does not capture drop coalescence effects.

Assumption $\mathbf{A}_1$ denotes that the spatial dynamics of a given plant ($\mathbf{H}_{l-1}$) are a function of previous layer topology ($\mathbf{g}_{l-1}$) and the surrounding environment. Assumption $\mathbf{A}_2$ holds for the additive system described in Eq. (2), given that material addition to the substrate is bounded by a predefined volume of available material. Furthermore, because of actuator constraints, the input in Eq. (2) is limited by an upper bound, ξ [13]. Assumption $\mathbf{A}_3$ simplifies the system dynamics for control design. The plant model is linear parameter-varying (LPV) integrator model of the heightmap evolution that captures the wetting nonlinearities, however, it still provides access to the linear control. Although many AM processes exhibit coalescence/surface effects that preclude linear superposition [16], [17], we capture these nonlinearities through model uncertainty in the plant model in Eq. (2).

IV. Higher-Order SILC for 3D Structures

In our prior work in [14], we derived a FO-SILC framework that used information from a previous device in the

device-axis (horizontal learning) to construct the feedforward input signal. In this work, we extend our previous framework by combining layer-to-layer learning (vertical direction) with device-to-device learning (horizontal learning) as presented in Figure 2. We term the proposed SILC algorithm higher-order SILC because learning occurs over one iteration in the device-axis (j, horizontal) and $\mathbf{N}$ iterations in the layer axis (l, vertical) as described in Figure 2. We will denote the order of the HO-SILC framework by bold variable $\mathbf{N}$ to distinguish it from the variables in Eq. (1).

For the multi-layer structure shown in Figure 2, a HO-SILC update law is proposed,

$$\mathbf{f}_{l,j+1} = (\mathbf{L}_f^h \mathbf{f}_{l,j} + \mathbf{L}_e^h \Delta\mathbf{e}_{l,j}) + \sum_{i=1}^{\mathbf{N}} (\mathbf{L}_f^{v_i} \mathbf{f}_{l-i,j+1} + \mathbf{L}_e^{v_i} \Delta\mathbf{e}_{l-i,j+1}) \quad (4)$$

with $\mathbf{L}_f^h$ and $\mathbf{L}_e^h$ defined as the horizontal input and error filters, respectively. $\mathbf{L}_f^{v_i}$ and $\mathbf{L}_e^{v_i}$ are vertical input and error filters for $i < l$. $\Delta\mathbf{e}_{l,j}$ is the incremental layer error calculated from the difference between the desired and actual height increments. To incorporate information from all of the printed layers, we choose $\mathbf{N} = \mathbf{L} - 1$, where $\mathbf{L}$ is the total number of layers to be printed. The incremental error, $\Delta\mathbf{e}_{l,j}$, is calculated from Eq. (3) as:

$$\Delta\mathbf{e}_{l,j} \triangleq \Delta\mathbf{g}^d - \Delta\mathbf{g}_{l,j} = \Delta\mathbf{g}^d - \mathbf{H}_{l-1,j}\mathbf{f}_{l,j} \quad (5)$$

A. Design of Learning Filters

Here, we implement a norm optimal-SILC (NO-SILC) algorithm [11] to design learning filters that are robust to model uncertainty. We define a weighted error vector, $\mathbf{e}^w_{l,j+1}$, as the following

$$\begin{aligned} &\mathbf{e}^w_{l,j+1} \triangleq \Delta\mathbf{e}_{l,j+1} + \alpha_1 \Delta\mathbf{e}_{l-1,j+1} + \ldots + \alpha_{\mathbf{N}} \Delta\mathbf{e}_{l-N,j+1} \\ &\vec{\alpha} \triangleq [1, \alpha_1, \alpha_2, \ldots, \alpha_N]^{\mathrm{T}} \end{aligned} \quad (6)$$

where $\alpha_i \in [0,1]$ are user defined HO-SILC parameters that weight the importance of previous layer errors. The quadratic cost function that for the HO-SILC filters is

$$\begin{aligned} &\mathscr{J} = \mathbf{e}^{w^T}_{l,j+1} \mathbf{Q} \mathbf{e}^w_{l,j+1} + (\mathbf{f}_{l,j+1} - \mathbf{f}_{l,j})^T \mathbf{R} (\mathbf{f}_{l,j+1} - \mathbf{f}_{l,j}) + \\ &\mathbf{f}^T_{l,j+1} \mathbf{S} \mathbf{f}_{l,j+1} + \sum_{i=1}^{\mathbf{N}} \beta_i (\mathbf{f}_{l,j+1} - \mathbf{f}_{l-i,j+1})^T \mathbf{R} (\mathbf{f}_{l,j+1} - \mathbf{f}_{l-i,j+1}), \end{aligned} \quad (7)$$

where $\mathbf{Q}$, $\mathbf{S}$, and $\mathbf{R} \in \mathbb{R}^{MN \times MN}$ are symmetric positive definite matrices that penalize the layer error, input signal, change in the input signal from iteration to iteration, and change in the input signal from layer to layer. Here we design weighting matrices as identity matrices multiplied by positive scalars q, s, and r such that $\mathbf{Q} = q\mathbf{I}$, $\mathbf{S} = s\mathbf{I}$, and $\mathbf{R} = r\mathbf{I}$; $\beta_i \in [0,1]$ are user defined parameters to weight the influence of previous layer input signals, such that $\vec{\beta} \triangleq [1, \beta_1, \beta_2, \ldots, \beta_N]^{\mathrm{T}}$. Note that if $\alpha_i = 1, \forall i$ in Eq. (6), and $\mathbf{N} = l - 1$, the cost function Eq. (7) is optimized over the total error (over l printed layers). In order to emphasize more recent layers, we set $\alpha_i = \frac{\alpha^i}{\|\vec{\alpha}\|}$ and $\beta_i = \frac{\beta^i}{\|\vec{\beta}\|}$, with $\alpha, \beta \in [0,1)$.

Applying the assumption of iteration invariant desired reference trajectories, we can relate two successive errors (iteration to iteration) within the same layer,

$$\Delta\mathbf{e}_{l,j+1} = \Delta\mathbf{e}_{l,j} + \mathbf{H}_{l-1,j}\mathbf{f}_{l,j} - \mathbf{H}_{l-1,j+1}\mathbf{f}_{l,j+1} \quad (8)$$

Substituting Eqs. (6) and (8) into Eq. (7) and setting the partial derivatives of $\mathscr{J}$ with respect to $\mathbf{f}_{l,j+1}$ equal to zero, the following relationships is obtained for the filters in Eq. (4) based on the nominal plant, $\mathbf{H}_0$,

$$\mathbf{L}_f^h = [\mathbf{H}_0^T \mathbf{Q} \mathbf{H}_0 + (\mathbf{S} + \mathbf{R} + \mathbf{R} \sum_{i=1}^{N} \beta_i)]^{-1} (\mathbf{H}_0^T \mathbf{Q} \mathbf{H}_0 + \mathbf{R}) \quad (9a)$$

$$\mathbf{L}_f^{v_i} = [\mathbf{H}_0^T \mathbf{Q} \mathbf{H}_0 + (\mathbf{S} + \mathbf{R} + \mathbf{R} \sum_{i=1}^{N} \beta_i)]^{-1} \mathbf{R} \beta_i \quad (9b)$$

$$\mathbf{L}_e^h = [\mathbf{H}_0^T \mathbf{Q} \mathbf{H}_0 + (\mathbf{S} + \mathbf{R} + \mathbf{R} \sum_{i=1}^{N} \beta_i)]^{-1} \mathbf{H}_0^T \mathbf{Q} \quad (9c)$$

$$\mathbf{L}_e^{v_i} = \mathbf{L}_e^h * \alpha_i \quad , i = 1, \ldots, \mathbf{N}. \quad (9d)$$

If the iteration varying spatial dynamics converge to the nominal model, $\lim_{l,j \to \infty} \mathbf{H}_{l,j} = \mathbf{H}_0$, the converged input would tend towards,

$$\mathbf{f}_\infty = [\mathbf{H}_0 (1 + \sum_{i=1}^{\mathbf{N}} \alpha_i) + (\mathbf{H}_0^T \mathbf{Q})^{-1} \mathbf{S}]^{-1} (\Delta\mathbf{g}_l^d + \sum_{i=1}^{\mathbf{N}} \alpha_i \Delta\mathbf{g}_{l-i}^d) \quad (10)$$

Under these conditions, the converged performance of the system is obtained by substituting Eq. (10) into Eq. (5),

$$\begin{aligned} \Delta\mathbf{e}_\infty = &(\mathbf{I} - [(1 - \sum_{i=1}^{\mathbf{N}} \alpha_i)\mathbf{I} + (\mathbf{H}_0^T \mathbf{Q})^{-1} \mathbf{S} \mathbf{H}_0^{-1}]^{-1}) \Delta\mathbf{g}_l^d \\ &- [(1 - \sum_{i=1}^{\mathbf{N}} \alpha_i)\mathbf{I} + (\mathbf{H}_0^T \mathbf{Q})^{-1} \mathbf{S}]^{-1} \sum_{i=1}^{\mathbf{N}} \alpha_i \Delta\mathbf{g}_{l-i}^d. \end{aligned} \quad (11)$$

B. *HO-SILC* Transformation To *FO-SILC*

HO-ILC processes generally achieve faster convergence as compared to FO-ILC, because HO-ILC uses information from multiple past trials to construct a more comprehensive input signal. However, in the ILC literature, there are few research papers that consider monotonic convergence (MC) of HO-ILC systems [18]. In comparison, the stability condition of FO-ILC is well described in [19]. In this section, we follow methods developed in [19]–[21] to convert the HO-SILC update law in Eq. (4) to a FO-SILC update law. Importantly, our approach requires a few additional considerations given the spatial dynamics and layer-to-layer interactions considered by HO-SILC and FO-SILC.

The HO-SILC algorithm defined in Eq. (4) can be expressed based on the closed-loop plant matrices by inserting Eq. (5) into Eq. (4) as,

$$\mathbf{f}_{l,j+1} = \mathbf{T}^h_{l-1,j} \mathbf{f}_{l,j} + \sum_{i=1}^{\mathbf{N}} \mathbf{T}^{v_i}_{l-i-1,j+1} \mathbf{f}_{l-i,j+1} + (\mathbf{L}_e^h + \sum_{i=1}^{\mathbf{N}} \mathbf{L}_e^{v_i}) \Delta\mathbf{g}^d \quad (12)$$

with $\mathbf{T}^h_{l,j} = \mathbf{L}_f^h - \mathbf{L}_e^h \mathbf{H}_{l,j}$ and $\mathbf{T}^{v_i}_{l-i,j} = \mathbf{L}_f^{v_i} - \mathbf{L}_e^{v_i} \mathbf{H}_{l-i,j}$ denoting the closed-loop horizontal and vertical plant matrices for $i \leq l$, respectively. Eq. (12) can be further simplified by concatenating the input signals over the vertical axis, l,

$$\begin{aligned} &\mathbf{z}_{l,j} = [\mathbf{f}^T_{l,j}, \ldots, \mathbf{f}^T_{2,j}, \mathbf{f}^T_{1,j}]^T \in \mathbb{R}^{lMN \times 1} \\ &\mathbf{z}_{l,j+1} = \mathbf{D}_{l,j} \mathbf{z}_{l,j} + \mathbf{K}_{l,j} \mathbf{z}_{l,j+1} + \mathbf{C}_l \\ &\mathbf{z}_{l,\infty} = (\mathbf{I} - \mathbf{D}_0 - \mathbf{K}_0)^{-1} \mathbf{C}_l \end{aligned} \quad (13)$$

where $\mathbf{D}_{l,j} \in \mathbb{R}^{lMN \times lMN}$ and $\mathbf{K}_{l,j} \in \mathbb{R}^{lMN \times lMN}$ are diagonal and upper triangular block matrices, and $\mathbf{C}_l \in \mathbb{R}^{lMN \times 1}$ is a constant vector. $\mathbf{z}_{l,\infty}$ is the converged input signal of the transformed FO-SILC system. $\mathbf{D}_0$ and $\mathbf{K}_0$ are nominal plant

matrices associated with the horizontal and vertical learning components of the update law.

$$\mathbf{D}_{l,j} = \begin{bmatrix} \mathbf{T}^h_{l-1,j} & \cdots & 0 \\ \vdots & \ddots & \vdots \\ 0 & \cdots & \mathbf{T}^h_{0,j} \end{bmatrix}, \mathbf{C}_l = \begin{bmatrix} \mathbf{L}^h_e + \mathbf{L}^{v_1}_e + \cdots + \mathbf{L}^{v_{l-1}}_e \\ \vdots \\ \mathbf{L}^h_e + \mathbf{L}^{v_1}_e \\ \mathbf{L}^h_e \end{bmatrix} \Delta \mathbf{g}^d$$

$$\mathbf{K}_{l,j} = \begin{bmatrix} \mathbf{0} & \mathbf{T}^{v_1}_{l-2,j+1} & \mathbf{T}^{v_2}_{l-3,j+1} & \cdots & \mathbf{T}^{v_{l-2}}_{1,j+1} & \mathbf{T}^{v_{l-1}}_{0,j+1} \\ & \mathbf{0} & \mathbf{T}^{v_1}_{l-3,j+1} & \cdots & \mathbf{T}^{v_{l-2}}_{1,j+1} & \mathbf{T}^{v_{l-2}}_{0,j+1} \\ & & \ddots & \ddots & \vdots & \vdots \\ \vdots & & & \mathbf{0} & \mathbf{T}^{v_1}_{1,j+1} & \mathbf{T}^{v_2}_{0,j+1} \\ & & & & \mathbf{0} & \mathbf{T}^{v_1}_{0,j+1} \\ \mathbf{0} & & & \cdots & & \mathbf{0} \end{bmatrix} \tag{14}$$

Eq. (13) can be further simplified to a FO-SILC format,

$$\begin{gathered} \mathbf{z}_{l,j+1} = \mathbf{F}_{l,j}\, \mathbf{z}_{l,j} + \mathbf{F}_r \\ \mathbf{F}_{l,j} = (\mathbf{I} - \mathbf{K}_{l,j})^{-1}\mathbf{D}_{l,j}, \quad \mathbf{F}_r = (\mathbf{I} - \mathbf{K}_{l,j})^{-1}\mathbf{C}_l \end{gathered} \tag{15}$$

We use the same notation as [19], [22] for transfer matrices $\mathbf{F}_{l,j}$ and $\mathbf{F}_r$. The FO-SILC algorithm in Eq. (15) will be used in the following section to investigate the asymptotic and monotonic properties of the HO-SILC update law in Eq. (12) leveraging methods described in [18], [19], [22].

V. Nominal Stability and Convergence

In most control systems, a fundamental goal is to guarantee the convergence of the tracking error to zero or within a neighborhood of a nominal value over a small number of iterations. In this section, we will combine the methods developed in [13], [18], [22] to derive nominal stability conditions for HO-SILC processes. Here we assume that the iteration varying plant model, $\mathbf{H}_{l,j}$, remains in a bounded neighborhood of the nominal plant, meaning $\|\mathbf{H}_{l,j} - \mathbf{H}_0\| \leq \kappa$ for a positive finite scalar κ and all $l, j \in \mathbb{N}$.

For the additive model in Eq. (2), the nominal plant matrix results from the desired topology, $\mathbf{H}_0 = \mathbf{H}(\mathbf{g}_d)$. The nominal matrices are:

$$\mathbf{D}_0 = \begin{bmatrix} \mathbf{T}^h_0 & \cdots & 0 \\ \vdots & \ddots & \vdots \\ 0 & \cdots & \mathbf{T}^h_0 \end{bmatrix}, \quad \mathbf{K}_0 = \begin{bmatrix} \mathbf{0} & \mathbf{T}^{v_1}_0 & \cdots & \mathbf{T}^{v_{l-2}}_0 & \mathbf{T}^{v_{l-1}}_0 \\ & \ddots & & & \vdots \\ & & & \mathbf{0} & \mathbf{T}^{v_1}_0 \\ \mathbf{0} & \cdots & & & \mathbf{0} \end{bmatrix} \tag{16}$$

In this case, the following properties are true:

- $\|\mathbf{D}_0\| = \|\mathbf{T}^h_0\|$
- $\|\mathbf{K}_0\|_1 \leq \sum_{i=1}^{\mathbf{N}} \|\mathbf{T}^{v_i}_0\|_1$
- $\|\mathbf{T}^h_0\| = \|\mathbf{L}^h_f - \mathbf{L}^h_e \mathbf{H}_0\|$
- $\|\mathbf{T}^{v_i}_0\| = \|\mathbf{L}^{v_i}_f - \mathbf{L}^{v_i}_e \mathbf{H}_0\|$

The second property has an equal sign for BCCB matrices.

Theorem 1: *The additive system in Eq.* (2) *controlled by the FO-SILC in Eq.* (15) *(or HO-SILC in Eq.* (4)*) is asymptotically stable for the nominal plant if and only if*:

$$\rho(\mathbf{T}^h_0) < 1, \tag{17}$$

where ρ is the spectral radius.

Proof: A nominal system representation of Eq. (15) is asymptotically stable using contraction mapping if $\rho(\mathbf{F}_0) < 1$, where $\mathbf{F}_0 = (\mathbf{I} - \mathbf{K}_0)^{-1}\mathbf{D}_0$. $(\mathbf{I} - \mathbf{K}_0)^{-1}$ is a strictly upper triangular block matrix with block-diagonal matrices equal to $\mathbf{I}$; therefore, the eigenvalues of $\mathbf{F}_0$ are equal to the eigenvalues of $\mathbf{D}_0$. $\mathbf{D}_0$ is a diagonal matrix and its spectral radius is equal to the spectral radius of the matrix $\mathbf{T}^h_0$. Therefore, the nominal system is stable if $\rho(\mathbf{T}^h_0) < 1$. ■

Although Theorem 1 provides a necessary condition for BIBO stability, it is not sufficient for ensuring an absence of large transient errors. In many manufacturing applications, such as the optical sensor presented in [2], large transient errors may introduce failures in the functional capabilities of the printed device. Therefore, the controller should be designed to regulate material deposition such that the layer errors decrease from iteration to iteration and layer to layer.

Theorem 2: *The additive system in Eq.* (2) *controlled by the FO-SILC in Eq.* (15) *is monotonically convergent for the nominal plant,* $\|\mathbf{Z}_{l,j+1} - \mathbf{Z}_{l,\infty}\| < \|\mathbf{Z}_{l,j} - \mathbf{Z}_{l,\infty}\|$*, if*:

$$\frac{1 - \|\mathbf{K}_0\|^{l-1}}{1 - \|\mathbf{K}_0\|} \times \|\mathbf{D}_0\| < 1, \quad \|\mathbf{F}_r\| < \xi, \tag{18}$$

where ξ is a positive scalar that ensures $\|\mathbf{F}_r\|$ remains bounded.

Proof: $\mathbf{K}_0$ is a strictly upper triangular block matrix containing block matrices of higher-order terms, $\mathbf{T}^{v_i}_0 \in \mathbb{R}^{MN \times MN}$, with l block zero matrices, $\mathbf{0} \in \mathbb{R}^{MN \times MN}$, along the diagonal. From linear algebra, $\mathbf{A}^l$ is zero for a strictly triangular matrix $\mathbf{A} \neq \mathbf{0} \in \mathbb{R}^{l \times l}$ with dimension l [23], [24]. We use this property for strictly upper triangular block matrix, $\mathbf{K}_0$, to avoid matrix inversion using the fact that $(\mathbf{K}_0)^l = \mathbf{0}$ (l here indicates layer number).

$$\mathbf{I} - \mathbf{K}^l_0 = (\mathbf{I} - \mathbf{K}_0)(\mathbf{I} + \mathbf{K}_0 + \mathbf{K}^2_0 + \ldots + \mathbf{K}^{l-1}_0) \tag{19}$$

which implies that

$$(\mathbf{I} - \mathbf{K}_0)^{-1} = (\mathbf{I} + \mathbf{K}_0 + \mathbf{K}^2_0 + \ldots + \mathbf{K}^{l-1}_0). \tag{20}$$

Using Eq. (20), the monotonicity condition is simplified to

$$\begin{aligned} \|\mathbf{F}_0\| &= \|(\mathbf{I} - \mathbf{K}_0)^{-1}\mathbf{D}_0\| \\ &= \|(\mathbf{I} + \mathbf{K}_0 + \mathbf{K}^2_0 + \ldots + \mathbf{K}^{l-1}_0)\mathbf{D}_0\| \\ &\leq (1 + \|\mathbf{K}_0\| + \|\mathbf{K}_0\|^2 + \ldots + \|\mathbf{K}_0\|^{l-1})\|\mathbf{D}_0\|. \end{aligned} \tag{21}$$

where the right side of Eq. (21) is a geometric sum that can be rewritten as $\frac{1-\|\mathbf{K}_0\|^{l-1}}{1-\|\mathbf{K}_0\|} \times \|\mathbf{D}_0\|$. The nominal representation of the FO-SILC in Eq. (15) is monotonically convergent if $\|\mathbf{F}_0\| \leq 1$. For $\frac{1-\|\mathbf{K}_0\|^{l-1}}{1-\|\mathbf{K}_0\|} \times \|\mathbf{D}_0\| < 1$, $\|\mathbf{F}_0\|$ will always be less than one. ■

Figure 3 shows the design regions of learning filters that correspond to $\mathrm{MC}_0 \triangleq \frac{1-\|\mathbf{K}_0\|^{l-1}}{1-\|\mathbf{K}_0\|} \times \|\mathbf{D}_0\| - 1$ for two different layer numbers, where negative values below a contour level of 0 relate to MC_0 stable regions for the nominal system. Note that if $\|\mathbf{K}_0\| << 1$, we can ignore $\|\mathbf{K}_0\|^{l-1}$ for higher layers and the monotonic stability region can be approximated by a line ($\|\mathbf{K}_0\| + \|\mathbf{D}_0\| < 1$). The area below the dashed red line represents an approximation

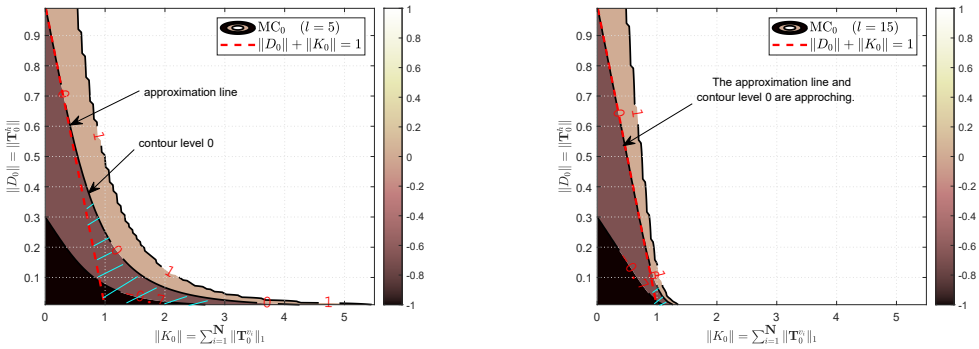

(a) stable region for $l=5$ (b) stable region for $l=15$

Fig. 3: **Monotonic nominal stability of HO-SILC**: the negative area below contour level **0** is related to the MC$_0$ stable regions for the nominal system. The area below the dashed red line is the approximated stable regions.

of the stable region defined by the MC$_0$ parameter. To ensure monotonicity, we design the learning filters such that $\|\mathbf{K}_0\|+\|\mathbf{D}_0\|<1$ (or $\|\mathbf{T}_0^h\|_1+\sum_{i=1}^{\text{L-1}}\|\mathbf{T}_0^{v_i}\|_1<1$). It can be seen that as the number of layers increases the area related to $\|\mathbf{K}_0\|+\|\mathbf{D}_0\|<1$ approaches the stable boundary condition deonoted by MC$_0=0$. Alternatively, as the number of layers decreases, $\|\mathbf{K}_0\|+\|\mathbf{D}_0\|<1$ becomes more conservative, as evident by the missing stable region shown with the dashed blue lines in Figure 3a.

VI. Simulation Setup

In this section, we apply the proposed HO-SILC framework to a simulation study using a model of an e-jet printing process. E-jet achieves material deposition using an electrostatic field, allowing for superior resolution and material diversity. Drop-on-demand printing is achieved using synchronized substrate motion and high voltage pulses applied to the nozzle tip of an e-jet printer, schematic shown in Figure 4a. Varying the rectangular wave pulse-width (while holding all other printing parameters constant) allows for variation in printed droplet size. The simulation assumes a known relationship between pulse-width and droplet size (cube root of droplet volume [16]).

For this simulation, the device structure has the topology given in Figure 2 with 100 nm layer heights for all layers. Each layer is printed in a single printing pass on top of a cured surface. The pitch size is set to 1 μm for a domain

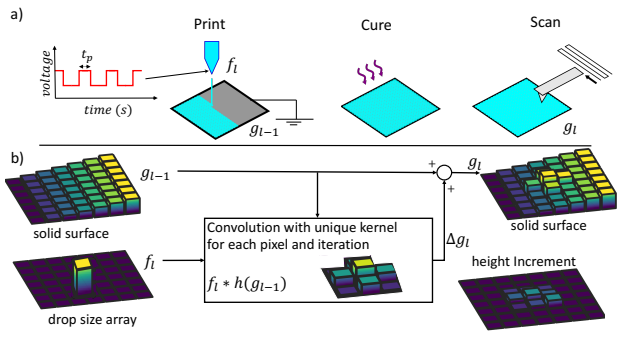

Fig. 4: **Heightmap evolution process**. a) Schematic of an e-jet printer: controlled device fabrication follows the print-cure-scan cycle. b) Evolution of the solid surface topology as a heightmap signal is modeled as the integration of a convolution of input f with kernel h.

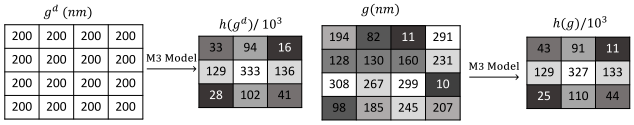

(a) Nominal model. (b) Effect of nonflat surface.

Fig. 5: **Topology dependent impulse response**. The estimated impulse response is spatially invariant (Method M3 of [16]), i.e. the same response for all spatial coordinates of g. Note that the estimated impulse response is iteration varying. a) Impulse of a flat surface. At left is a 4×4 pixel crop of reference topology signal. At right is the 3×3 corresponding impulse response. b) Impulse of a nonflat surface. At left is a 4×4 pixel of a spatially varying g signal. At right is the 3×3 corresponding impulse response.

of 256×256 pixels. The desired output, g^d, is uniform except for the ten outer rings of pixels, which are reduced by half to better represent material drop-off at the edges. Heightmap evolution from layer-to-layer is simulated according to Eq. (1) and depicted in Figure 4b. $h_{l-1}^{(m,n)}$ describes the spreading behavior of a printed material on the neighboring coordinates for an input signal with magnitude one applied at coordinate (m,n) and layer $l-1$.

The dependence of $h_{l-1}^{(m,n)}$ on existing topology g_l is modeled using the multivariate regression method (method M3) from [16]. Method M3 results in a less accurate model than other methods in [16]; however, the plant matrix associated with M3 is BCCB. In this method, numerical simulations of droplets spreading to equilibrium on nonflat surfaces are precomputed for an equilibrium contact angle associated with a specific material/substrate combination: 15° for the ink (NOA170) used in this simulation. Subsequently, an ordinary least squares multivariate linear regression is performed, where the elements from each 3×3 pixel crop of the heightmap g are the predictor variables, and the elements from each measured 3×3 pixel impulse response h are the response variables. The fitted regression model is used to evaluate the spatially varying impulse response $h_{l-1}^{(m,n)}$ for the 3×3 pixel crop of the heightmap g_l centered at pixel coordinates (m,n), as shown in Figure 4b and Figure 5b. Taking an average of $h_{l-1}^{(m,n)}$ over all spatial coordinates results in a spatially invariant impulse response.

The nominal model, h_0, is calculated by evaluating the impulse response for a uniform reference topology g_d, as shown in Figure 5a. In contrast, an example of an impulse

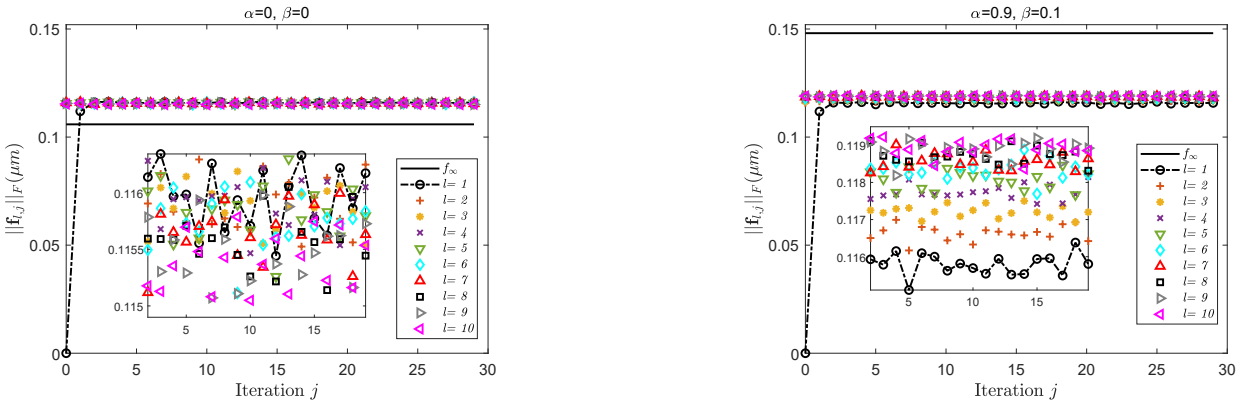

(a) Input signal of FO-SILC approaches a nominal value over iterations.

(b) Input signal of HO-SILC approaches a nominal value over iterations.

Fig. 6: **Convergence of SILC:** $(\alpha,\beta)=(0,0)$ refer to FO-SILC which only has horizontal learning. $(\alpha,\beta)=(0.9,0.1)$ refer to HO-SILC which integrates horizontal learning from device to device with vertical learning from previous layers. Iteration $j=0$ refers to the first device. ($q=1$, $r=0.01$, $s=0.03$).

response prediction for a non-flat surface is provided in Figure 5b. The impulse response $h_{l,j}$ is used to derive the plant matrix $\mathbf{H}_{l,j}$ in Eq. (2).

VII. Simulation Results

In this section, simulation results of the system described in Section III using HO-SILC are investigated. A multi-layer structure with $\mathrm{L}=10$ layers is considered (Figure 2). Note that a selection of $\beta=0$ and $\alpha=0$ results in a FO-SILC update law [14]. To satisfy $\|\mathbf{K}_0\|+\|\mathbf{D}_0\|<1$, we set $\beta=0.1$ and $\alpha=0.9$ for the HO-SILC update law. This results in $\|\mathbf{D}_0\|=\|\mathbf{T}_0^h\|=0.1612$ and $\|\mathbf{K}_0\|_1=\sum_{i=1}^{\mathbf{L-1}}\|\mathbf{T}_0^{v_i}\|_1=0.7363$. Note that in this case, $\mathrm{MC}_0=0.5724$.

It is important to note that the inputs of the first iteration at the first layer are zero, $\mathbf{f}_{1,1}=\mathbf{0}$, implying that there is no prior knowledge of the appropriate inputs. This results in no material being deposited during the first iteration of the first layer. However, the input of the first device at higher layers, $l\geq 2$, comes from the last device in the previous layer, such that $\mathbf{f}_{l,1}=\mathbf{f}_{l-1,J}$ where J is the total number of iterations. In e-jet printing, droplet volume has a standard variation of 25% over a wide range of droplet sizes [25]. Therefore; a normally distributed white noise with variance of 0.25 μm is added to the input signal such that $\Delta\mathbf{g}_{l,j}=\mathbf{H}_{l-1,j}\mathbf{f}_{l,j}\circ(\mathbf{1}_{MN\times 1}+\mathscr{N}(0,0.25^2)_{MN\times 1})$, where $\circ$ denotes Hadamard product and $\mathbf{1}$ is a vector of ones. The input will be constrained to positive definite values to ensure an additive process.

Figures 6a and 6b show the Frobenius norm of the input signal for FO-SILC and HO-SILC frameworks. The input signal generated by the FO-SILC update law converges to the nominal input with approximately the same offset at all layers. On the other hand, the HO-SILC framework results in monotonic convergence of the input to the nominal input over the layers. The nominal input signal is slightly larger for HO-SILC based on the higher-order coefficients in Eq. (10).

Figures 7a and 7b present the Frobenius norm of the incremental errors, $\Delta\mathbf{e}_{l,j}$. Figure 7a shows that the final incremental errors of the FO-SILC update law are in the same range over the layers. Figure 7b shows that by using HO-SILC a significant improvement in the incremental error over the layers is achieved. The first layer shows the highest error, with the error signals decreasing due to vertical learning through the iterations.

Figure 8 shows that HO-SILC demonstrates improvement in overall performance (smaller total heightmap error) when compared to FO-SILC. Larger values of α impose more weighting on previous layer errors in Eq. (6) that results in smaller total errors, $\mathbf{e}_{l,j}$. This is consistent with the performance metric in Eq. (11) for an ideal case where the system behavior converges to the nominal state. On the other hand, when considering the iteration varying system provided in Eq. (2), larger values of β result in an increase in the total error, especially for higher layers where the variation between the nominal plant model and true plant dynamics is more pronounced. As such, the higher-order control terms associated with β result in a reduction of system robustness.

VIII. Conclusion

In this paper, we present a higher-order spatial ILC framework for iterative systems with an application to additive manufacturing processes. In multi-layer structures that are fabricated using AM technologies, errors in previous layers are compounded over multiple layers, resulting in significant distortions of the final printed component. The proposed HO-SILC framework combines device-to-device learning with layer-to-layer learning to generate a feedforward signal that addressed error propogation over layers. Simulation results of an e-jet printing system demonstrate that HO-SILC can be successfully employed in AM processes to regulate the input of an iterative model and improve the heightmap reference tracking. Higher order SILC has applications outside of additive manufacturing systems. For example, any system that exhibits spatially dependent dynamics through a repetitive action (e.g. exoskeletons, robotic pick and place) could benefit from a control framework that compensates for errors across both a spatial and temporal domain. Importantly, spatial interactions are often disjointed temporally and are commonly ignored. The proposed framework addresses this issue by incorporating spatial information into the control law. Future work will focus on stability of spatially and iteration varying HO-SILC framework to determine the maximum

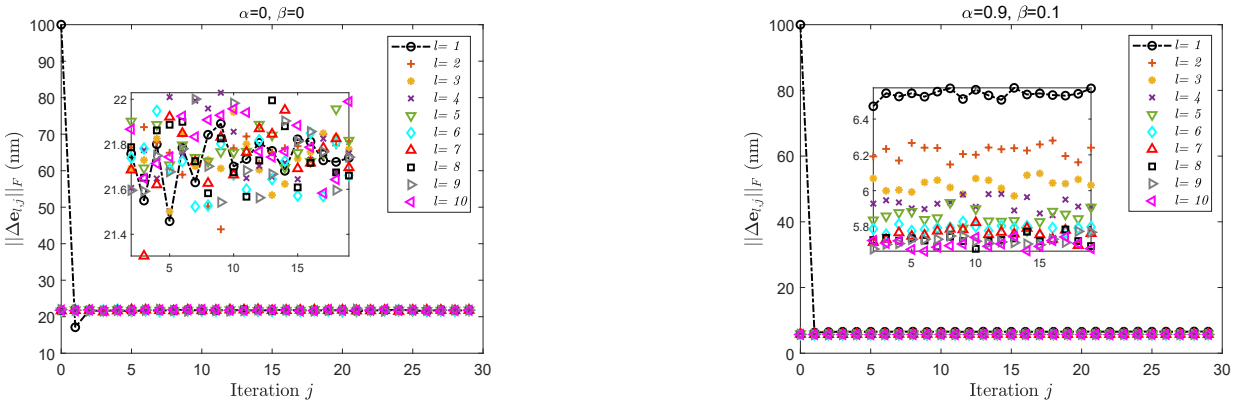

(a) Frobenius norm of the incremental error.

(b) Frobenius norm of the incremental error.

Fig. 7: **Convergence of SILC**: $(\alpha,\beta)=(0,0)$ refer to FO-SILC which only has horizontal learning. $(\alpha,\beta)=(0.9,0.1)$ refer to HO-SILC which integrates horizontal learning from device to device with vertical learning from previous layers. HO-ILC offers better performance over the layers compared to the FO-SILC. Iteration $j=0$ refers to the first device. ($q=1$, $r=0.01$, $s=0.03$).

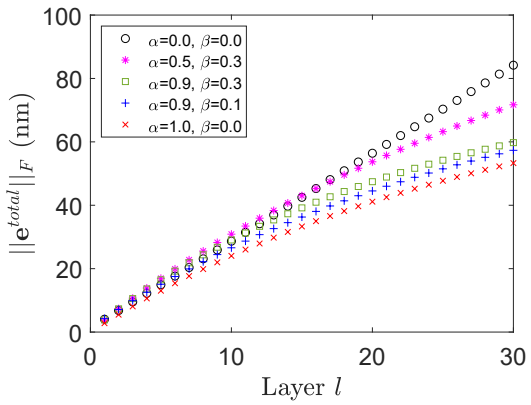

Fig. 8: **Total error comparison**: HO-SILC results in a lower total error compared to FO-SILC. $\alpha=0$ and $\beta=0$ refer to FO-SILC, which only has horizontal learning (iteration to iteration). ($q=1$, $r=0.01$, $s=0.03$).

allowable uncertainty around the nominal plant such that the iterative system remains stable. In addition, future work will include implementation of HO-SILC on an experimental platform.

References

[1] I. Gibson, D. Rosen, and B. Stucker, *Additive manufacturing technologies: 3D printing, rapid prototyping, and direct digital manufacturing, second edition*, 2015.

[2] B. Iezzi *et al.*, "Electrohydrodynamic jet printing of 1d photonic crystals: Part ii—optical design and reflectance characteristics," *Advanced Materials Technologies*, vol. 5, p. 2000431, 2020.

[3] P. M. Theiler, F. Lütolf, and R. Ferrini, "Non-contact printing of optical waveguides using capillary bridges," *Opt. Express*, 2018.

[4] Y. Wang, F. Gao, and F. J. Doyle, "Survey on iterative learning control, repetitive control, and run-to-run control," 2009.

[5] X. Bu, F. Yu, Z. Fu, and F. Wang, "Stability analysis of high-order iterative learning control for a class of nonlinear switched systems," in *Abstract and Applied Analysis*, vol. 2013. Hindawi, 2013.

[6] Y.-S. Wei and X.-D. Li, "Robust higher-order ilc for non-linear discrete-time systems with varying trail lengths and random initial state shifts," *IET Control Theory & Applications*, vol. 11, pp. 2440–2447, 2017.

[7] Z. Bien and K. M. Huh, "Higher-order iterative learning control algorithm," in *IEE Proceedings D (Control Theory and Applications)*, vol. 136, no. 3. IET, 1989, pp. 105–112.

[8] Y. Chen, Z. Gong, and C. Wen, "Analysis of a high-order iterative learning control algorithm for uncertain nonlinear systems with state delays," *Automatica*, vol. 34, pp. 345–353, 1998.

[9] M. Q. Phan and R. W. Longman, "Higher-order iterative learning control by pole placement and noise filtering," *IFAC Proceedings Volumes*, vol. 35, pp. 25–30, 2002.

[10] S. S. Saab, "On higher-order iterative learning control algorithm in presence of measurement noise," in *Proceedings of the 44th IEEE Conference on Decision and Control*. IEEE, 2005, pp. 2451–2456.

[11] D. J. Hoelzle and K. L. Barton, "On Spatial Iterative Learning Control via 2-D Convolution: Stability Analysis and Computational Efficiency," *IEEE Trans. Control Syst. Technol.*, 2016.

[12] Z. Wang *et al.*, "An application of spatial iterative learning control to micro-additive manufacturing," in *2016 American Control Conference (ACC)*. IEEE, 2016, pp. 354–359.

[13] B. Altin, Z. Wang, D. J. Hoelzle, and K. Barton, "Robust Monotonically Convergent Spatial Iterative Learning Control: Interval Systems Analysis via Discrete Fourier Transform," 2018.

[14] Z. Afkhami *et al.*, "Spatial iterative learning control for multi-material three-dimensional structures," *ASME Letters in Dynamic Systems and Control*, vol. 1, 2020.

[15] L. Aarnoudse *et al.*, "Multi-layer spatial iterative learning control for micro-additive manufacturing," *IFAC-PapersOnLine*, vol. 52, pp. 97–102, 2019.

[16] C. Pannier, M. Wu, D. Hoelzle, and K. Barton, "LPV models for jet-printed heightmap control," in *2019 Amer. Control Conf.* Philadelphia, PA: IEEE, 2019.

[17] C. P. Pannier *et al.*, "An electrohydrodynamic jet printer with integrated metrology," *Mechatronics*, vol. 56, pp. 268–276, dec 2018.

[18] H.-S. Ahn, K. L. Moore, and Y. Chen, *Iterative learning control: robustness and monotonic convergence for interval systems*. Springer Science & Business Media, 2007.

[19] M. Norrlöf and S. Gunnarsson, "Time and frequency domain convergence properties in iterative learning control," *Int. J. Control*, 2002.

[20] N. Amann, D. H. Owens, and E. Rogers, "2d systems theory applied to learning control systems," in *Proceedings of 1994 33rd IEEE Conference on Decision and Control*, vol. 2. IEEE, 1994, pp. 985–986.

[21] E. Rogers and D. H. Owens, *Stability analysis for linear repetitive processes*. Springer, 1992, vol. 175.

[22] M. Norrlof and S. Gunnarsson, "A frequency domain analysis of a second order iterative learning control algorithm," in *Proceedings of the 38th IEEE Conference on Decision and Control (Cat. No. 99CH36304)*, vol. 2. IEEE, 1999, pp. 1587–1592.

[23] A. Cayley, "A memoir on the theory of matrices." *Proceedings of the Royal Society of London Series I*, vol. 9, pp. 100–101, 1857.

[24] T. Crilly, "Cayley's anticipation of a generalised cayley-hamilton theorem," *Historia Mathematica*, vol. 5, pp. 211–219, 1978.

[25] D. J. Hoelzle and K. L. Barton, "A new spatial iterative learning control approach for improved micro-additive manufacturing," in *2014 American Control Conference*. IEEE, 2014, pp. 1805–1810.